Two-Dimensional Inversion of Papua New Guinea Magnetotelluric Dataset Assuming Static Shift as a Gaussian Distribution

Yasuo Ogawa[1,2]

[1] Geological Survey of Canada, 1 Observatory Crescent, Ottawa, Ontario K1A 0Y3, Canada
[2] Geological Survey of Japan, 1-1-3 Higashi, Tsukuba, Ibaraki 305, Japan

The Papua New Guinea Magnetotelluric dataset was analyzed by applying Groom-Bailey tensor decomposition, and a consistent strike direction of N66°W was determined. The dataset was approximated by two-dimensional impedances, and frequency independent twist and shear. The static shift parameters (local anisotropy and site gain) were determined using a two-dimensional inversion where static shifts were also part of the model parameters. The model misfit was simultaneously minimized together with the following two norms: (1) roughness norm of the model, and (2) static shift $L2$ norm. The trade-off parameters between the model misfit and these norms were determined so as to minimize the Akaike's Bayesian Information Criterion (ABIC).

1. Introduction

The Papua New Guinea (PNG) magnetotelluric (MT) dataset was made available to the induction community by Charley Swift of Chevron. The survey was carried out for the purpose of petroleum exploration. The region is characterized by the resistive Darai limestone covering the conductive sediments which are potential hydrocarbon resources. This is a difficult area for seismic reflection surveys, due to the reflective limestone cover together with access difficulties, and thus MT is an alternative to seismic methods. The purpose of this study was to apply recent techniques to the dataset, and to refine the model with special reference to the location of limestone.

The dataset consists of 10 wideband magnetotelluric sites, and is discussed by Jones and Schultz (1997). The profile was designed across believed geological strike for the area, and the site separations range from 200 m to 1200 m. The frequency (period) ranges are from 384 Hz down to 1820 s, however, some of the data with periods longer than 100 s show large errors and could not be used. The magnetic transfer function data were of poor quality and therefore were not used in the two-dimensional modeling.

2. Decomposition of Tensor Impedances

In the presence of near surface structures, the telluric fields are often distorted. Conventional analyses (Swift, 1967) may give misleading strike directions, as well as inaccurate impedances and dimensionality. The tensor impedances were decomposed into parameters descriptive of the near surface distortion and the regional two-dimensional induction. The observed impedances Z can be decomposed into the following equation after Groom and Bailey (1989),

$$Z = R(\theta) \begin{bmatrix} 1 & -t \\ t & 1 \end{bmatrix} \begin{bmatrix} 1 & e \\ e & 1 \end{bmatrix} g \begin{bmatrix} 1+s & 0 \\ 0 & 1-s \end{bmatrix} Z_{2d} R(-\theta) \qquad (1)$$

where θ, $R(\theta)$, t, e, g, and s are the strike direction, rotation matrix, the twist, the shear, the site gain, and the local anisotropy, respectively. Z_{2d} is the two-dimensional impedances that are

composed of off-diagonal elements.

2.1 Determining strike directions

First, the regional strike was estimated by Groom-Bailey (G-B) decomposition. The distortion parameters (twist, shear, and strike direction) are site-dependent and frequency-dependent. The histograms of the estimated strike directions are shown in Fig. 1 for each decade of frequency, where each strike estimated from a single frequency at a single site contributes equally (in the figure, π and $\pi/2$ ambiguities are also shown). Clear preference of the regional strike was found around WNW, especially in the period range longer than 1 s. The alternative strike direction (around NNE) is rejected based on the prior knowledge that the geological strike is close to WNW. In the shorter period range (100 Hz $\sim$ 1 Hz) the strike estimates scatter, probably reflecting local structures.

For the next stage, a site-independent strike was sought for the subsequent two-dimensional modeling. Since the interest lies in the deep structure below the surface cover, the analyses were carried out for the three decades of period from 1 s to 1000 s. The decomposition was done for each decade of period using both site-independent frequency-independent strike and site-dependent frequency-independent twist and shear, as detailed by McNeice (1994) and McNeice and Jones (1996). The inverse of variance was used as the weight in the calculation. The estimated regional strikes for each decade of frequency were N57±2°W (1 $\sim$ 10 s), N66±8°W (10 $\sim$ 100 s), and N72 ± 8°W (100 $\sim$ 1000 s). This implies that there is a strike dependency with respect to
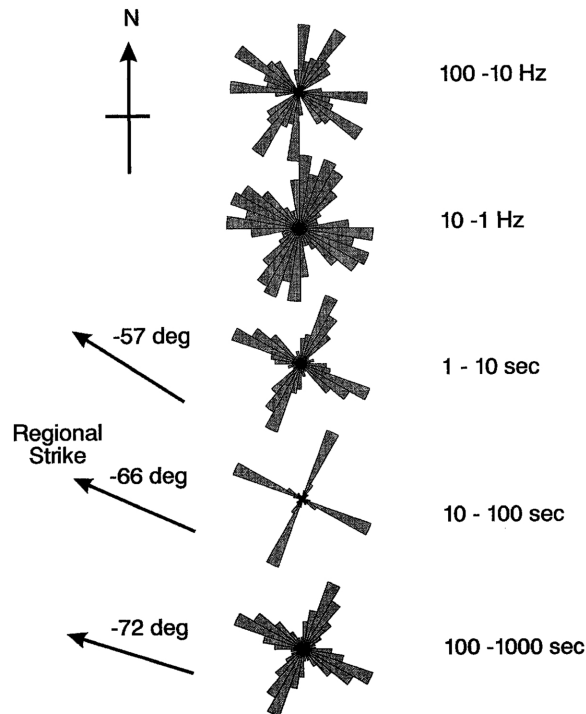

Fig. 1. Rose diagrams showing the histograms of the regional strikes estimated from all of the ten sites, using the unconstrained decomposition method of Groom and Bailey (1989). For each decade of frequencies, the size of the diagram is normalized by the maximum histogram. For the three longest period decades, survey-consistent strike was estimated using the algorithm of McNeice (1994) and McNeice and Jones (1997).

depth. The error data for the PNG data set is given by the algorithm of Stodt (1981) which could be underestimated for shorter periods and overestimated for longer periods (Chave and Jones, 1997). If we take all period bands together, the strike will be dominated by the shorter periods. To avoid this, throughout the following analyses, a strike of N66°W from the period band 10–100 s was used.

2.2 Constrained decomposition

After fixing the regional strike as N66°W, all the impedance tensors were again decomposed with frequency-independent twist and shear. This means that the dataset was approximated by the distortion model with 3D surface distortion. However, in the decomposition, the G-B parameters g, s, and Z_{2d} are not uniquely solved. The following Z'_{2d} is obtained as a unique impedance matrix rather than Z_{2d}.

$$Z'_{2d} = g \begin{bmatrix} 1+s & 0 \\ 0 & 1-s \end{bmatrix} Z_{2d} = \begin{bmatrix} 0 & g_{\mathrm{TE}}Z_{\mathrm{TE}} \\ -g_{\mathrm{TM}}Z_{\mathrm{TM}} & 0 \end{bmatrix}. \tag{2}$$

The factors to Z_{2d} represent the so-called static shifts. Without any additional data or assumptions, these shift parameters (g_{TE} and g_{TM}) cannot be solved. Here an assumption is introduced that the static shift will follow a Gaussian distribution (Ogawa and Uchida, 1996), i.e., smaller static shifts are assumed to be more likely. The apparent resistivity and phase from the Z'_{2d} are plotted in Fig. 6 together with the two-dimensional inversion responses which will be described later.

3. Introducing Two Norms: Model Roughness and Static Shift

Two-dimensional inversion was applied to the decomposed data set based on that of Ogawa and Uchida (1996), described briefly below.

The model was constructed using rectangular finite elements grouped into regularization blocks (Fig. 2). The static shifts were taken as model parameters similar to those described by deGroot-Hedlin (1991). Therefore, the model parameters m are written as follows:

$$m = \begin{bmatrix} m_{\rho,\mathrm{block}} \\ g_{\mathrm{site,mode}} \end{bmatrix} \tag{3}$$

where $m_{\rho,\mathrm{block}}$ denotes the $\log_{10}$(resistivity) of the regularization blocks. Model misfit is defined as follows:

$$S(m) = |Wd - WF(m)|^2 \tag{4}$$

where d, W, and F denote data, reciprocal of the standard error of the data, and function mapping a model into the data space, respectively. S can be approximated by S_0 as shown below using the model parameters of the previous iteration m_{old} and a Jacobian matrix A.

$$S(m) \approx S_0(m) = \left| W\tilde{d} - WAm \right|^2 \tag{5}$$

where,

$$\tilde{d} = d - F(m_{\mathrm{old}}) + Am_{\mathrm{old}}. \tag{6}$$

S_0 (instead of S) was minimized under the constraints of the following two norms.

The first norm is model roughness, defined as R as follows:

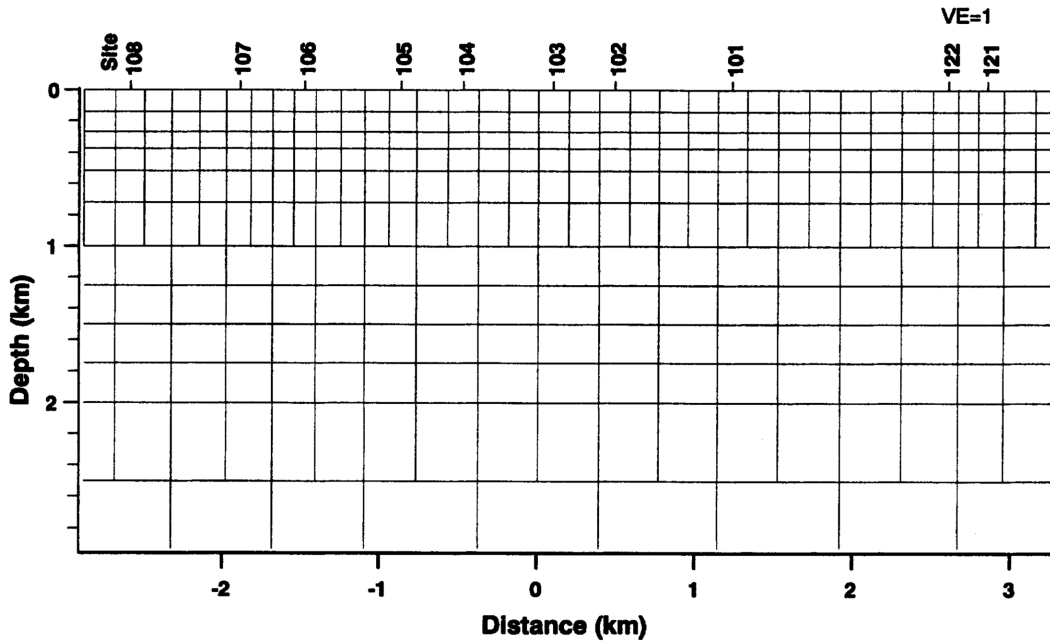$$R = |C_v m_\rho|^2 + |C_h m_\rho|^2. \tag{7}$$

Fig. 2. Regularization grids for the two-dimensional inversion.

The first and second terms denote the vertical and horizontal roughness, respectively. Matrix C_v is composed of coefficients so that the i-th row of $C_v m_\rho$ represents the difference between the $\log_{10}$(resistivity) of the i-th regularization block and the average of the neighboring vertical blocks. Likewise, matrix C_h is composed of coefficients so that the i-th row of $C_h m_\rho$ represents the difference between the $\log_{10}$(resistivity) of the i-th regularization block and the average of the neighboring horizontal blocks. Note here, that the shape of the regularization block is not reflected in the design of the C_v nor the C_h matrices. Thus, the design of the regularization grid reflects a *prior* knowledge (prejudice) about the model.

In comparison, Uchida (1993a, b) defined roughness as follows:

$$R_u = |(C_v + C_h)m_\rho|^2 \tag{8}$$

which is a Laplacian roughening. This means that the roughness is calculated from the difference between the i-th block $\log_{10}$(resistivity) and that of the whole of the neighboring blocks. Within this roughness definition, the model can have saddle points (i.e., the i-th block is a peak vertically and a trough horizontally) without increasing the roughness norm in Eq. (8). In this paper, roughness definition of Eq. (7) was used.

The second norm is the static shift $L2$ norm, G, defined as follows:

$$G = \sum |\log_{10} g_{\text{site,mode}}|^2. \tag{9}$$

In the paper of deGroot-Hedlin (1991), the following norm (sum of the static shift) was forced to be zero.

$$G_{dh} = \sum \log_{10} g_{\text{site,mode}}. \tag{10}$$

If the number of data is large enough (however we never know if the number of data is really

large enough), G_{dh} could be forced to be zero. Thus, in this study a constraint was made so that G could be kept to minimum.

4. Bayesian Statistics

In Bayesian statistics, the probability density function of the whole data d with regard to model m is as follows:

$$p(d|m) = \left(2\pi\sigma^2\right)^{-N/2} \exp\left(-\frac{S_0}{2\sigma^2}\right) \qquad (11)$$

where N is the number of the data. σ is the variance and can also be thought of as the correction factor to the estimated standard error. Note that S_0 is quadratic related to m because of the linear approximation in Eq. (5).

Next, we assume that both model roughness and static shift follow a Gaussian distribution. The former assumption was also assumed by Uchida (1993a, b), and the latter is a reasonable assumption, as field data (Sternberg et al., 1988; Kurtz and Gupta, 1992) suggested that more occurrences for smaller static shifts exist. Thus, the prior distribution of the model is as follows:

$$\pi(d|m) = D\left(2\pi\sigma^2\right)^{-N/2} \exp\left(-\frac{\alpha^2 R}{2\sigma^2} - \frac{\beta^2 G}{2\sigma^2}\right) \qquad (12)$$

where D is a normalizing factor when $\pi(m)$ is integrated over the whole model space. The likelihood of the data is written as L which is a function of σ, α, and β.

$$L(\alpha, \beta, \sigma) = \int p(d|m)\pi(m)dm. \qquad (13)$$

Note that both $p(d|m)$ and $\pi(m)$ have quadratic terms in the argument for their exponentials and can be easily calculated (see Ogawa and Uchida, 1996, for more details). Given α and β, L is maximized with the following σ:

$$\sigma^2 = \frac{1}{N} \min\left(S_0 + \alpha^2 R + \beta^2 G\right). \qquad (14)$$

With the maximized L value, ABIC is defined as a function of α and β (Akaike, 1980; Uchida, 1993a, b).

$$\text{ABIC}(\alpha, \beta) = -2\log(\max L) + 2(\text{dimension of hyper parameters}). \qquad (15)$$

The minimum value of ABIC (as a function of α and β) can be obtained by a direct numerical search, as described by Murata (1993).

5. Result of Two-Dimensional Inversion

The algorithm outlined was applied to the decomposed (but not static shift corrected) PNG dataset. Ten frequencies were used in the inversion over the whole period range. However, only a couple of sites had meaningful data below 0.01 Hz. The error floor for the apparent resistivity data was set to 10%, which will flatten the smallest error distribution at around 1.5 Hz. An equivalent error was set for phase. The regularization blocks were designed as shown in Fig. 2. The model has both ends 200 km away from the edges of the model shown in Fig. 2. The starting model was a uniform earth of 100 Ω·m resistivity.

Two hyper parameters α and β were numerically sought to minimize the ABIC for each iteration. The rms and best hyper parameters, estimated at each iteration, are plotted in Figs. 3(a) and 3(b). After the 14-th iteration, rms reached a value of 0.83 and the next iteration did not
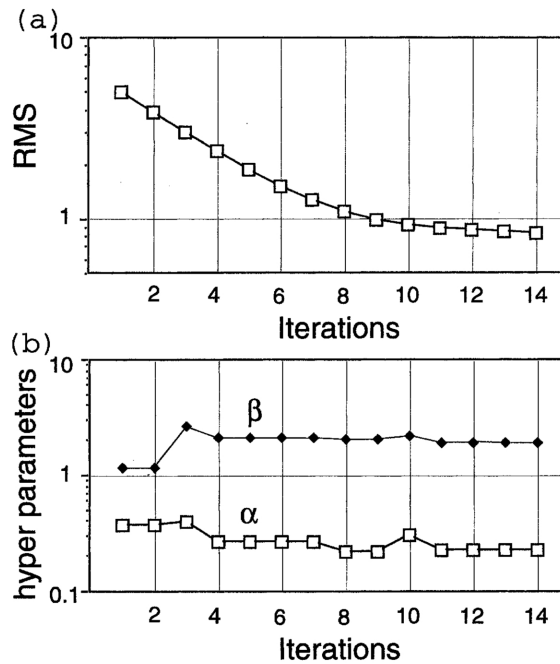
Fig. 3. (a) rms as a function of the iterations, (b) hyper parameters α and β as functions of the iterations.

significantly decrease the rms (less than 1 %). At the final iteration, minimizing L in Eq. (13) lead to $\sigma = 0.41$. From Eq. (11), this means that the correct standard deviation of the data should be further multiplied by 0.41. Thus, the small rms value of 0.83, which means overfitting, is due to the overestimation of the standard error of the data.

Figure 4 shows the static shift parameters analyzed by this inversion. The changes of the static shift with respect to the iteration were plotted for both TM and TE modes. The amplitudes of TE mode static shifts increase with the increasing iterations, whereas the TM mode distributions are not as simple. The standard deviation of the $\log_{10}$(static shift) is predicted as $\sigma/\beta = 0.22$, referring to Eq. (12), which is consistent with the mean $L2$ norm of the estimated static shifts in Figs. 4(a) and 4(b).

Figure 5(a) illustrates the final model. The model responses, which include static shifts, are plotted in Fig. 6. Note, that the error floor is not taken into account in the plots of the observed data. As seen in Fig. 6, a reasonable fit was obtained.

For the confirmation of the model features, comparative calculations using TM-only, and TE-only inversions were performed. The results are shown in Figs. 5(b) and (c). The TM-only and the TE-only inversions give simple structures compared to the TM+TE case. The complex structure in Fig. 5(a) is the result of inverting both modes simultaneously.

The roughness of the structure was defined for shallow (<0.5 km) and deep structures (>0.5 km), separately. The threshold depth of 0.5 km was chosen, because it is approximately the typical skin depth for the highest frequency (384 Hz) and the corresponding typical apparent resistivity (300 $\Omega\cdot$m). Corresponding to shallow roughness (R_1) and deep roughness (R_2), two hyper parameters α_1 and α_2 were introduced instead of the single α parameter. The idea is to treat shallow structures, which have a strong interaction with the static shift parameters, in a
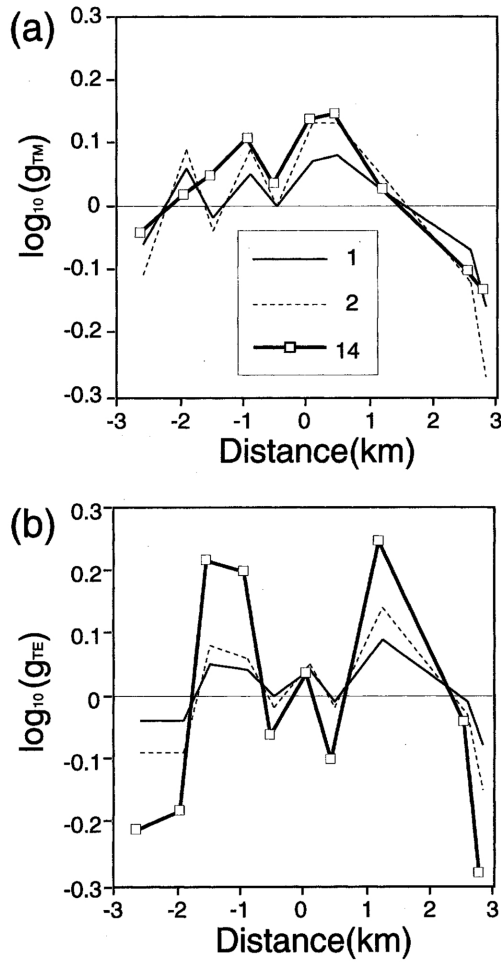
Fig. 4. Distribution of static shift factors for (a) TM and (b) TE modes, respectively. The numbers in the legend boxes denote the iterations.

special way. Thus, the prior distribution of the model (Eq. (12)) is modified as follows:

$$\pi(d|m) = D(2\pi\sigma^2)^{-N/2} \exp\left(-\frac{\alpha_1^2 R_1}{2\sigma^2} - \frac{\alpha_2^2 R_2}{2\sigma^2} - \frac{\beta^2 G}{2\sigma^2}\right). \qquad (16)$$

Three hyper parameters α_1, α_2 and β were numerically sought to minimize the ABIC for each iteration. The result of the three hyper parameter case is shown in Fig. 5(d). However, by introducing three parameters, there are no major differences in the corresponding models.

6. Implications of the Model

The major features in the final model (Fig. 5(a)) have the following implications. At sites 101 and 102, there is a surface conductive cover over the resistive structure (>300 Ω·m). To the left of these sites, the resistive unit is exposed at sites 105–108. Thus, the resistive layer is dipping beneath sites 104–101. This resistive structure implies the distribution of the Darai limestone
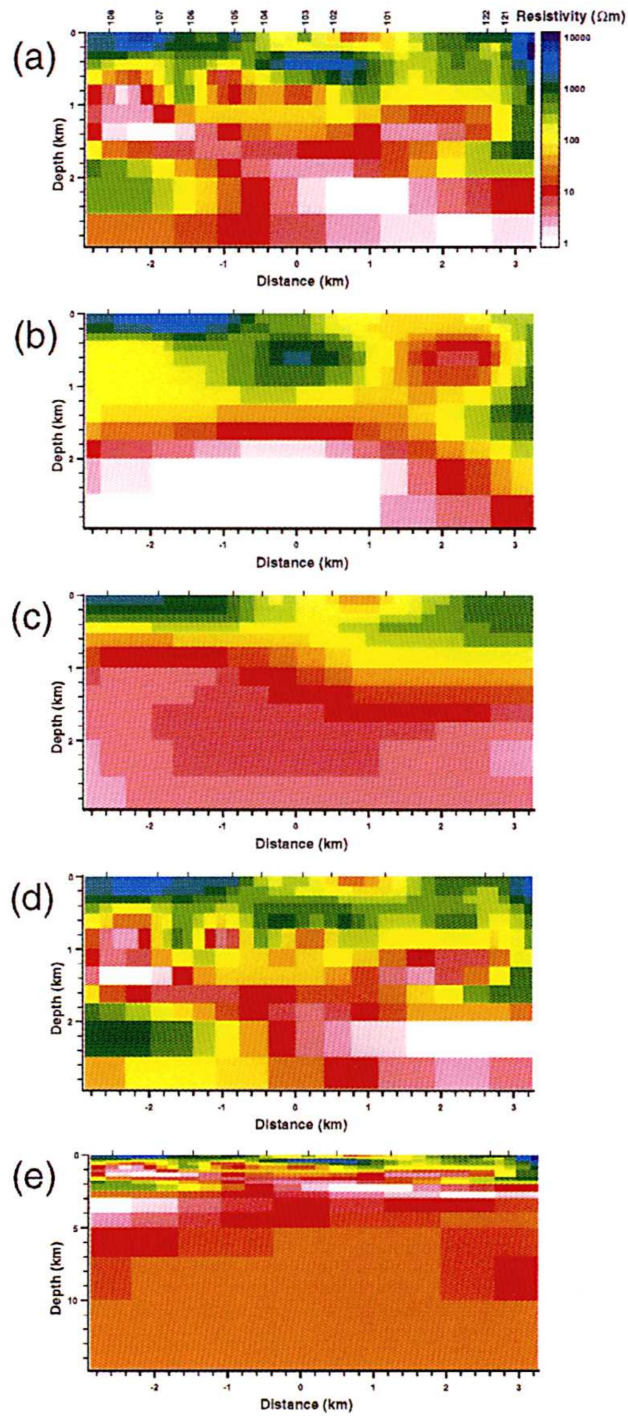
Fig. 5. Final resistivity model from the inversion. (a) two hyper parameter case using the TM and TE modes, (b) two hyper parameter case using the TM mode only, (c) two hyper parameter case using the TE mode only, (d) three hyper parameter case using the TM and TE modes, (e) deeper structure of model (a).
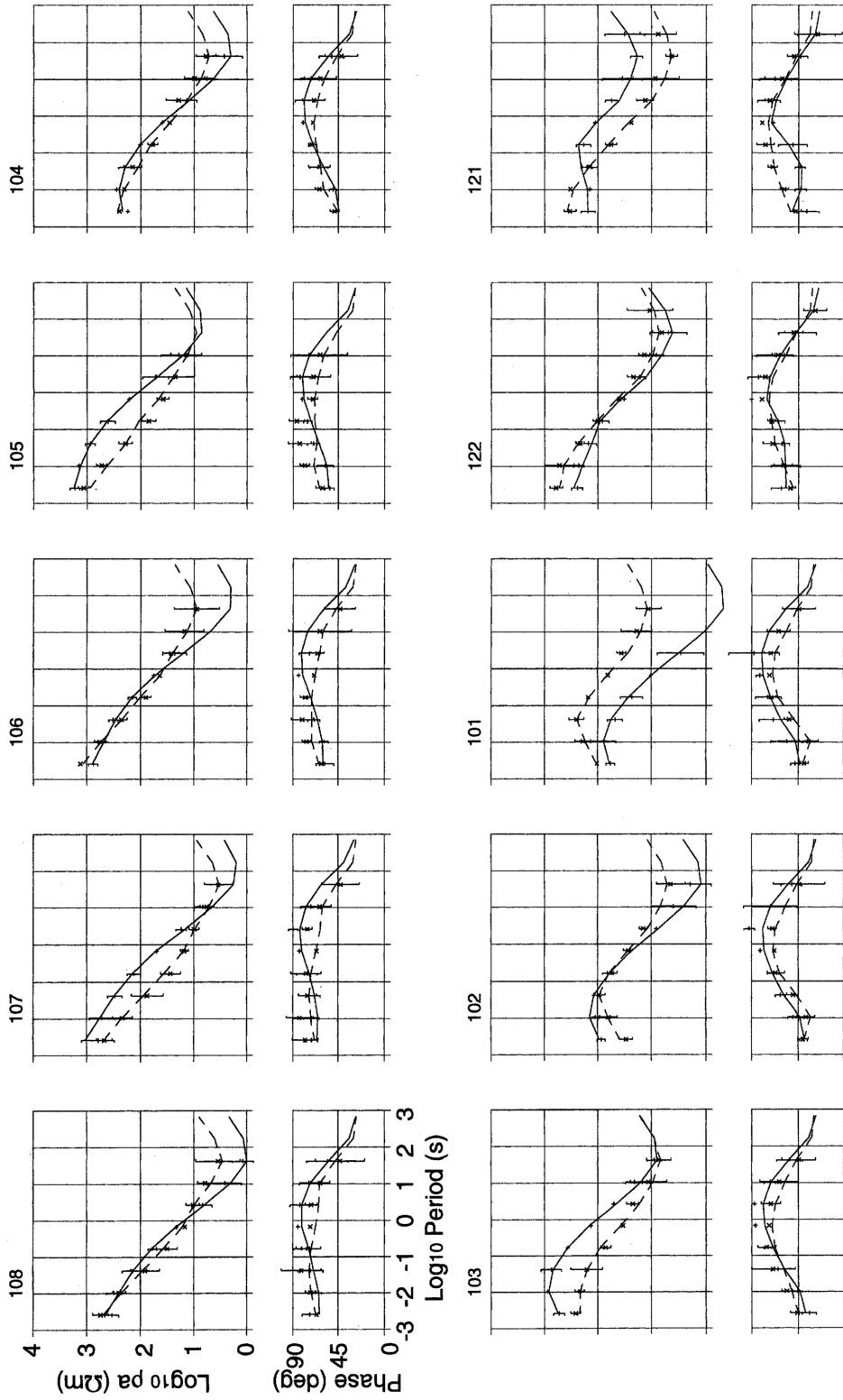
Fig. 6. Decomposed data with a dataset-consistent strike direction (N66°W). The plus and cross denote the decomposed data for TM and TE modes, respectively. The error floor used for the inversion is not taken into account in the plots. The solid and broken lines denote the theoretical responses (i.e. including static shifts) for the TM and TE modes, respectively.

(Jones and Schultz, 1997). The resistive unit is underlain by a very conductive layer beneath all of the sites. The top of the conductor is shallow (~0.6 km depth) beneath sites 107–108, 105, and 103. Note that the surface conductor at sites 101–102 is not connected to the deeper conductor.

Beneath the conductor, there is a resistive zone only between sites 107 and 108 at 1.7–2.5 km depth. This implies another thusted sheet of the Darai limestone. However, the lateral extension further to the right beyond these sites was not detected. This means that the deep thrust sheet composed of the Darai limestone does not completely underlie the survey profile, which supports the single Darai model, rather than the double Darai model (Jones and Schultz, 1997).

Figure 5(e) shows the deeper structures of the model shown in Fig. 5(a). All the sites did not have good data for the long periods (>100 s). The usable data shows an increase of the apparent resistivity towards the long periods, as seen in the responses at sites 121 and 122 (Fig. 6). The corresponding structure is the underlying resistive layer beneath the conductive layer, which appears to be an anticline feature.

7. Conclusions

Tensor decomposition can solve the phase mixing between the tensor elements, but it cannot solve the static shift problem. To remove the static shift, additional information or assumptions are necessary. In this study, static shift was assumed to follow a Gaussian distribution. Two-dimensional inversion was conducted using two kinds of constraints as described by Ogawa and Uchida (1996). One constraint is model roughness, and the other is the static shift $L2$ norm. The trade-off parameters between misfit and the constraints were chosen so that Akaike's Bayesian Information Criterion (ABIC) is minimized. This algorithm worked well to find a reasonable misfit, as well as proper model roughness and static shifts. It also helped estimates for the correction factor for the given errors in the field data. Finally, the resulting model obtained suggests that the single Darai model is more likely to be correct, rather than the double Darai model.

REFERENCES

Akaike, T., Likelihood and Bayes procedure, in *Bayesian Statistics*, edited by J. M. Bernardo, M. H. deGroot, D. V. Lindley, and S. F. Smith, pp. 143–166, University press, Valencia, 1980.

Chave, A. D. and A. G. Jones, Electric and magnetic field galvanic distortion decomposition of BC87 data, *J. Geomag. Geoelectr.*, **49**, this issue, 767–789, 1997.

deGroot-Hedlin, C., Removal of static shift in two dimensions by regularized inversion, *Geophys.*, **56**, 2102–2106, 1991.

Groom, R. W. and R. C. Bailey, Decomposition of magnetotelluric impedance tensor in the presence of local three-dimensional galvanic distortion, *J. Geophys. Res.*, **94**, 1913–1925, 1989.

Jones, A. G. and A. Schultz, Introduction to MT-DIW2 special issue, *J. Geomag. Geoelectr.*, **49**, this issue, 727–737, 1997.

Kurtz, R. D. and J. C. Gupta, Shallow and deep crustal conductivity studies in the Miramichi earthquake zone, New Brunswick, *Can. J. Earth Sci.*, **29**, 1549–1564, 1992.

McNeice, G. W., Magnetotelluric investigation of the Appalachian orogen, Msc. Thesis, Memorial Univ. of Newfoundland, Newfoundland, Canada, 1994.

McNeice, G. W. and A. G. Jones, Multi-site, multi-frequency tensor decomposition of magnetotelluric data, Expanded Abstracts with biographies, SEG International Exposition and 66th Annual meeting, Technical program Volume I, 281–284, 1996.

Murata, Y., Estimation of optimum average surficial density form gravity data: An objective Bayesian approach, *J. Geophys. Res.*, **98**, 12,097–12,109, 1993.

Ogawa, Y. and T. Uchida, A two-dimensional magnetotelluric inversion assuming Gaussian static shift, *Geophys. J. Int.*, **126**, 69–76, 1996.

Sternberg, B. K., J. C. Washburne, and L. Pellerin, Correction for the static shift in magnetotellurics using transient electromagnetic soundings, *Geophys.*, **53**, 1459–1468, 1988.

Stodt, J., Algorithm for magnetotelluric calculations in the frequency domain, 103 pp., Phoenix Geophysics, Denver, 1981.

Swift, C. M., A magnetotelluric investigation of an electrical conductivity anomaly in the southern United States., Ph.D. Thesis, Dep. of Geol. and Geophys., Mass. Inst. of Technol., Cambridge, 1967.

Uchida, T., Smooth 2-D inversion for magnetotelluric data based on statistical criterion ABIC, *J. Geomag. Geoelectr.*, **45**, 841–858, 1993a.

Uchida, T., Inversion of COPROD2 magnetotelluric data by use of ABIC minimization method, *J. Geomag. Geoelectr.*, **45**, 1063–1071, 1993b.